Remote Spatio-Temporal Focusing Over Multimode Fiber Enabled by Single-Ended Channel Estimation

Haoshuo Chen, Nicolas K. Fontaine, Roland Ryf, David T. Neilson, *Fellow, IEEE*, and Peter Winzer, *Fellow, IEEE*

(Invited Paper)

***Abstract*—Multimode fiber (MMF) is attractive for a variety of applications requiring a large number of spatially overlapped modes including biophotonics and telecommunications. Superimposing these modes at the input by controlling the amplitude and phase of each individual mode can form arbitrarily structured light at the distal end of the MMF, which provides the possibility for ultra-thin fiber endoscopy, miniature multi-photon microscopy, and remote beam forming. Realistic deployment of this technology for example in a flexible endoscope would require a technique to continuously calculate the proper input modal superpositions over a large bandwidth as the fiber is perturbed without access to the distal end of the fiber. Here, we propose a single-ended channel estimation scheme which can measure broad-band MMF transfer matrix H at the transmitter employing reflective spatial pilots at the distal end of the MMF. Broadband multiple-input-multiple-output (MIMO) preprocessing is realized through electro-optic modulation for undoing mode scrambling, mitigating modal dispersion and achieving remote coherence control. We demonstrate spatial and temporal mode focusing at the receiver over an MMF guiding six spatial and polarization modes.**

***Index Terms*—Mode division multiplexing, digital signal processing, coherence control, channel estimation, endoscopy.**

I. Introduction

ULTRA-THIN optical fiber-based endoscopy shows great potential in minimally invasive in vivo imaging [1]–[5]. Diffraction-limited spatial resolution and 50 μm field of view can be realized employing a multimode fiber (MMF) with a diameter of 60 μm in deep brain in vivo imaging [5]. To use the MMF as an imaging system, fiber needs to be pre-calibrated to measure mode coupling, which results in light launched in one input mode arriving in multiple output modes due to perturbations to the waveguide structure, as illustrated in Fig. 1(a). These can arise from imperfections in fiber fabrication such as refractive index non-uniformity and diameter fluctuations, or environmentally through temperature variations, fiber bending, twisting, and stretching. Fiber needs to keep rigid during the whole imaging process. Any perturbation, which changes mode coupling, will result in a fiber re-calibration, which makes current MMF-based endoscopy experience limited flexibility. A perturbation-insensitive MMF-based endoscopy requires a solution to continuously measure the fiber coupling matrix without access to the distal end of the fiber.

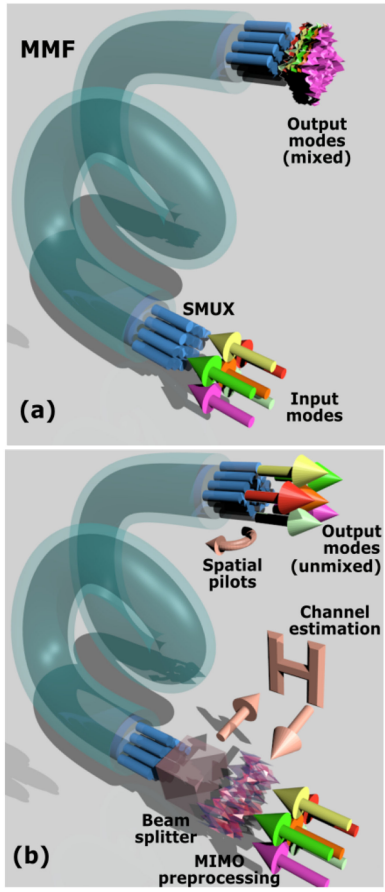

Fig. 1. Illustrations of (a) mode mixing after propagation over MMF, (b) remote mode focusing employing transmitter-side MIMO preprocessing and single-ended channel estimation.

In addition to mode coupling, different propagation constants or modal dispersion result in different time delays for light coupling between modes. In mode-division multiplexed communication systems [6], [7], all of the modal dispersion, and mode

Manuscript received October 16, 2019; revised February 5, 2020; accepted February 6, 2020. Date of publication March 9, 2020; date of current version March 25, 2020. *(Corresponding author: Haoshuo Chen.)*

The authors are with the Nokia Bell Labs, Holmdel, NJ 07733 USA (e-mail: haoshuo.chen@nokia-bell-labs.com; nicolas.fontaine@nokia-bell-labs.com; roland.ryf@nokia.com; david.neilson@nokia-bell-labs.com; peter.winzer@ieee.org).

Color versions of one or more of the figures in this article are available online at http://ieeexplore.ieee.org.

Digital Object Identifier 10.1109/JSTQE.2020.2979241

mixing is numerically reversed at the receiver using multiple-input-multiple-output (MIMO)-based digital signal processing (DSP). Receiver-side MIMO-DSP techniques usually employ pilot symbols as part of the transmitted information stream to determine the fiber's N inputs to N outputs transfer matrix $\mathbf{h}$ and $\mathbf{H}$, respectively in time and frequency domain, for a fiber supporting N spatial and polarization modes. Once $\mathbf{H}$ is known, the transmitted information stream can be reconstructed from the coherently detected information stream through a simple matrix inversion (or through a matrix of filters).

MIMO processing can also be performed at the input end of the fiber (i.e., at the transmitter), by programming each spatial input with the proper amplitude and phase such that the individual modes superimpose in the desired manner at the fiber output. In a communications context, this is done by first determining the transfer matrix $\mathbf{H}$ through pilot symbols, communicating the estimated $\mathbf{H}$ back to the transmitter, and digitally pre-compensating for back-propagating the desired output field to the fiber input to determine the modal launch conditions. This ensures that the output signal appear both temporally (i.e., without dispersion) and spatially in the desired manner at the fiber output. Typically there are environmental changes for the fiber which results in $\mathbf{H}$ changing, which means it must be continuously measured and adapted to. The DSP can deal with large modal dispersion which causes $\mathbf{H}$ to change rapidly with wavelength and cause temporal defocusing which is represented by adding a frequency dimension to $\mathbf{H}$.

Compared to receiver-side MIMO, transmitter-side MIMO removes almost all complexity from the receiver and can find uses in passive optical networks (PON) where the head-end can be complex, but the receivers must be kept extremely simple and inexpensive [8]–[10]. This potentially expands the opportunities for space division multiplexing in cost-sensitive short-reach and in-building optical-wireless networks based on an existing MMF infrastructure and requiring low-cost and simple receiver schemes. A major challenge in implementing transmitter-side MIMO is that it requires the knowledge of the frequently updated transfer matrices over a certain bandwidth.

Outside of telecommunication, transmitter-side MIMO processing is sometimes called digital phase conjugation for narrow-band signals [11]–[15] or "time-reversal" for broadband signals [16]–[19] because the proper launched fields are computed by propagating the desired output fields backwards in time to the input. These schemes are necessary for the MMF-based endoscopy [1]–[5] and miniature multiphoton microscopy [20], [21], which focuses light at the distal end. Time reversal techniques require estimation of the fiber transfer matrix $\mathbf{H}$ over a certain bandwidth [14], [15]. Up till now, measuring the complex $\mathbf{H}$ required access to both fiber facets and a lengthly calibration procedure that sequentially launches each mode and measures the spatial output. Such measurement is not possible in real applications where the matrix is continuously changing as the fiber is perturbed and when the distal end is remote and not accessible. Single-ended measurements of $\mathbf{H}$ have been proposed theoretically [22] but have not been demonstrated.

This paper is extended from our previous work [23], [24] and organized as follows: Section II introduces a single-ended channel estimation scheme and employs the proposed scheme to measure the transfer matrices of different optical fibers. Section III discusses broadband transmitter-side MIMO preprocessing and presents experimental results about spatio-temporal focusing over MMF. Section IV concludes the paper.

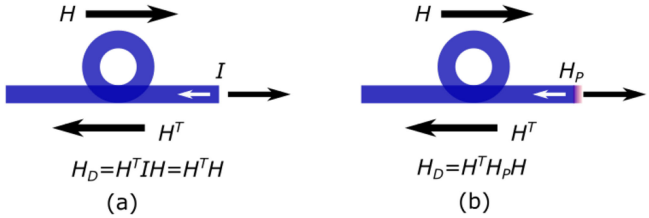

Fig. 2. Double-pass matrix $\mathbf{H_D}$ in single-ended channel estimation as (a) all the modes are simply reflected due to facet reflection and (b) each spatial and polarization mode is coded using reflective spatial pilots $\mathbf{H_P}$.

II. Single-Ended Channel Estimation

A. Spatial Pilots

Transfer matrix $\mathbf{H}(f)$ of an MMF, representing forward propagation of N spatial and polarization modes from proximal end to distal end, is with a dimension of N-by-N-by-M, where f is the frequency and M is the number of frequency samples. As all the modes exit the fiber at the distal end into free space, portion of the light will be reflected backward due to Fresnel reflection. This facet reflection matrix $\mathbf{I}$ can be treated as an identity matrix, where no mode mixing occurs for all the modes. The transfer matrix for backward propagation can be expressed as $\mathbf{H}^T$ because of reciprocity [22], where ^{T} is the transpose operator. Then the double-pass matrix $\mathbf{H_D}$, undergoing forward propagation, facet reflection and backward propagation, can be formatted as $\mathbf{H}^T\mathbf{I}\mathbf{H}$. Here, we will answer why $\mathbf{h}$ or $\mathbf{H}$ cannot be extracted from simply reflecting all the modes using facet reflection, see Fig. 2(a). It is known that the multiplication between a real unitary matrix and its transpose produces an identity matrix: $\mathbf{U}\mathbf{U}^T = \mathbf{U}^T\mathbf{U} = \mathbf{I}$. Therefore, it can be rewritten as $\mathbf{H_D} = \mathbf{H}^T\mathbf{U}^T\mathbf{U}\mathbf{H} = (\mathbf{U}\mathbf{H})^T(\mathbf{U}\mathbf{H})$, which indicates that the solution is not unique and any real unitary matrix times $\mathbf{H}$ could be the solution.

To realize single-ended $\mathbf{H}$ estimation, we propose to partially reflect all the modes back to the input end after being passively encoded with different information, named as spatial pilots, at the remote-end spatial multiplexer (SMUX). After employing the spatial pilots, the double pass matrix $\mathbf{H_D}$ can then be expressed as $\mathbf{H^T H_P H}$, see Fig. 2(b), where $\mathbf{H_P}$ is a diagonal matrix, whose diagonal elements represent the spatial pilots coded onto different modes. In this paper, we will focus on using different time delays to passively encode the spatial pilots at the distal end [23], [24] and the diagonal elements of $\mathbf{H_P}$ are expressed as $s_1 = e^{j2\pi f t_1}$, $s_2 = e^{j2\pi f t_2}$, ..., $s_N = e^{j2\pi f t_N}$, where t_1 to t_N are the different time delays added to different modes. Other domains such as frequency and power can also be applied for the encoding.

$\mathbf{H_D}$ can be decomposed into N separate matrices, whose diagonal elements can be used to calculate the N elements

Algorithm 1: $H_{Reconst}(H_D(f), H_P(f), M, N)$.

```
for j in M do
    H_D = H_D(f_j)
    for i in N do
        Resolve H_{s_i} at t_i
        Calculate |H_{i1}|, |H_{i2}|, ..., |H_{iN}| using diag(H_{s_i})
        Correct relative phase between H_{i1}, H_{i2}, ..., H_{iN}
        with non-diag(H_{s_i})
    end for
end for
```

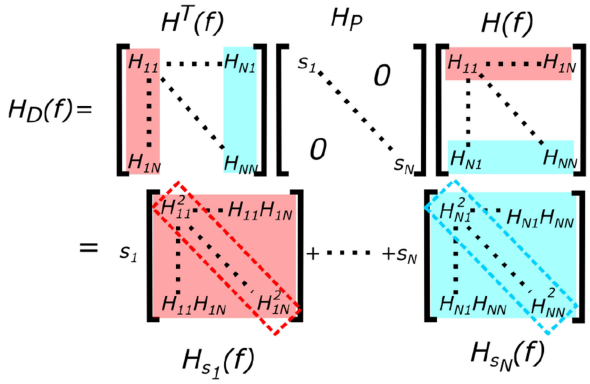

Fig. 3. Illustrations of reconstructing transfer matrix $\mathbf{H}(f)$ from N time-resolved N-by-N matrices ($\mathbf{H_{s_1}}(f), \ldots, \mathbf{H_{s_N}}(f)$), separated from double pass matrix $\mathbf{H_D}$ using spatial pilots $s_1, \ldots, s_N$.

in each row of $\mathbf{H}$, as illustrated by different colors in Fig. 3. The non-diagonal elements are used to correct the π phase ambiguity between the N elements arising from the square root operation, see Algorithm 1. For example, the amplitudes of $H_{11}, H_{12}, \ldots, H_{1N}$, which are the 1^{st} row of $\mathbf{H}$ at each frequency bin, can be calculated by taking the square roots of the diagonal elements of the N-by-N matrix $\mathbf{H_{s_1}}$, resolved at t_1. The elements at the 1^{st} column of $\mathbf{H_{s_1}}$ are $H_{11}^2, H_{11}H_{12}, \ldots, H_{11}H_{1N}$, which provide the relative phase relations between the elements $H_{11}, H_{12}, \ldots, H_{1N}$ and can properly correct the π phase ambiguity.

The only remaining inaccuracy is the π phase ambiguity between the rows of $\mathbf{H}$, which is yet to be determined in the single-ended measurements since either 0 or π phase difference becomes an integer of 2π after passing through the fiber twice. Spatio-temporal focusing each mode only relies on the elements within each row of $\mathbf{H}$ and has no requirement for the absolute phase between the rows of $\mathbf{H}$. The phase ambiguity between the rows of $\mathbf{H}$ can be avoided by measuring the interference between the modes at the proximal side, which can be accomplished by adding an additional partial reflector at the distal end.

B. Measurement Results

We employed a swept-wavelength interferometry with polarization diversity [25] to characterize $\mathbf{H}(f)$ of different optical fibers. Fig. 4 shows the setup for characterizing an SMF, a polarization maintaining fiber (PMF) and an MMF supporting LP_{01} and $LP_{11a/b}$ modes. Fiber delays were added at the input and

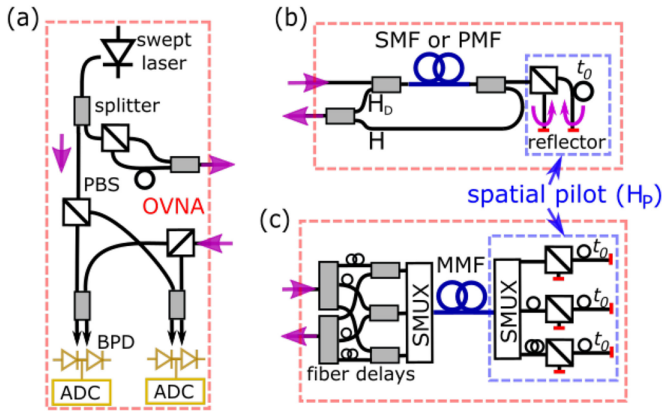

Fig. 4. (a) Setup of the swept-wavelength interferometry, link for characterizing, (b) an SMF and PMF, and (c) an MMF supporting 6 spatial and polarization modes.

output of the swept-wavelength interferometer to differentiate all the transmitted and received spatial and polarization modes in time domain. Fiber loop mirrors were used as reflectors. As both fiber facets are accessible, N-by-N fiber transfer matrix $\mathbf{H}$ can be measured directly. In single-ended measurements, spatial pilots are added at the distal end and N temporally spaced N-by-N impulse-response matrices are measured. To verify the accuracy of $\mathbf{H}$ reconstruction using the spatial pilots, element-wise matrix intensity and phase comparisons between directly measured $\mathbf{H}$ and reconstructed $\mathbf{H}$ from $\mathbf{H_D}(f)$ in the frequency range from 192 THz to 196 THz are presented in Fig. 5(a). Negligible reconstruction errors can be observed from both intensity and phase differences after correcting the π phase ambiguity due to the square root operation. Fig. 5(b) shows the reconstructed $\mathbf{H}$ of a 2-m PMF covering the 4-THz bandwidth, where large polarization modal dispersion (PMD) can be observed. The result of a 3-m graded-index MMF [26] guiding 6 spatial and polarization modes ($LP_{01x,y}$, $LP_{11ax,y}$ and $LP_{11bx,y}$) is presented in Fig. 5(c), which gives the intensity of summed $\mathbf{H}$ over the 4-THz measured bandwidth. Mode group separation can be observed due to the usage of a pair of mode-group selective SMUX [27] and negligible coupling between the mode groups from the short MMF.

III. Remote Spatio-Temporal Focusing

By applying the inverted transfer matrix $\mathbf{H^{-1}}$ to the transmitted signal, mode coupling after transmission is eliminated, giving the transmitter full control over the individual fiber modes at the remote end. Different propagation velocities for different modes and mode coupling cause modal (polarization) dispersion in optical fiber, which induces $\mathbf{H}$ varying over the frequency. In order to focus light pulses or modulated signals which occupy a broad frequency range, broadband MIMO preprocessing is required based on the knowledge of time-resolved $\mathbf{h}(t)$ or frequency-resolved $\mathbf{H}(f)$.

It is challenging to directly sample the light pulses and do time reversal operation at optical domain [17], which requires fast sampling at optical frequency and usually introduces huge losses

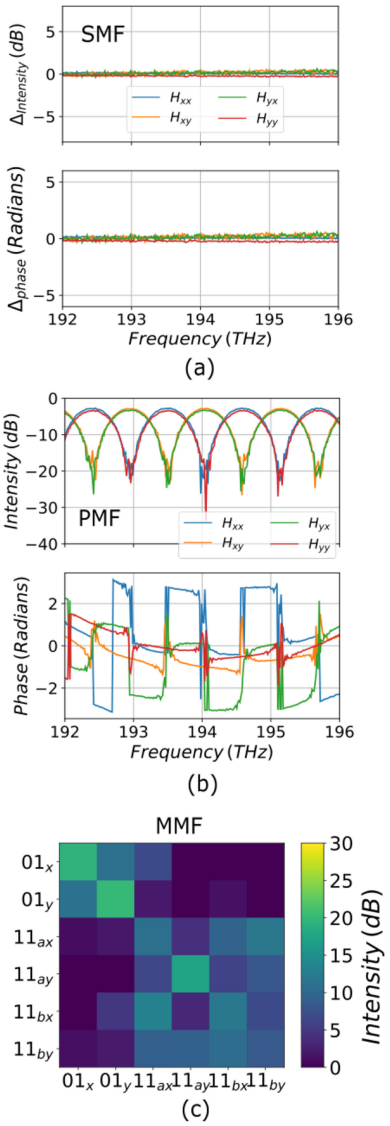

Fig. 5. (a) Element-wise matrix intensity and phase comparisons between directly measured $\mathbf{H}$ and reconstructed $\mathbf{H}$ from $\mathbf{H_D}(f)$, reconstructed $\mathbf{H}$ for (b) a PMF and (c) an MMF supporting 6 spatial and polarization modes.

due to light splitting and combining. In the field of telecommunication, time reversal has an analogy to transmitter-side MIMO processing through an array of transmitters. Employing optical modulators, time reversal can be operated within the signal bandwidth instead of at the carrier frequency [16]. Time reversal over an SMF has been demonstrated [18], [23] employing electro-optic modulation and we have shown the possibility to remotely focus two polarization states in parallel over a 5-km SMF [23]. PMD after short-distance SMF transmission is comparably small so dispersion induced inter-symbol interference (ISI) is usually negligible and an equalizer with a single tap is sufficient to undo polarization mixing. Modal dispersion in either a polarization maintaining fiber (PMF) or an MMF can be ten times larger than that in an SMF and its compensation requires an equalizer with multiple taps at the receiver. Therefore, transmitter-side MIMO preprocessing needs to handle frequency-dependent $\mathbf{H}$ as a broadband operation.

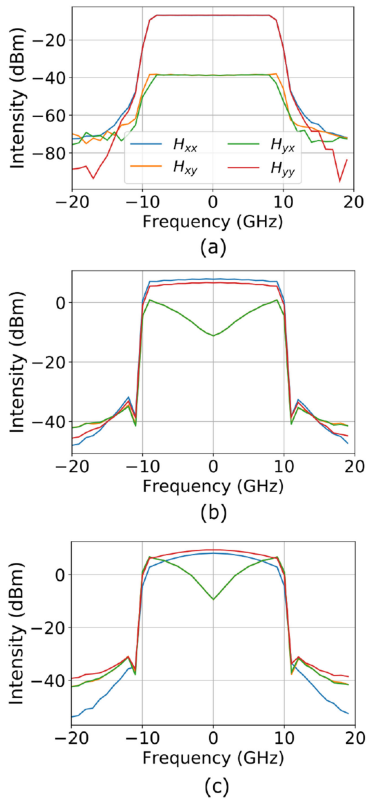

Fig. 6. Simulation results for the intensity of all four elements of $\mathbf{H_{MD}H^{-1}}$ using (a) full frequency-resolved transfer matrices $\mathbf{H^{-1}}(f)$ as broadband MIMO preprocessing, (b) and (c) only $\mathbf{H^{-1}}(f=0)$ as the polarization delay is 20 ps and 40 ps, respectively, as narrow-band MIMO preprocessing.

A. *Broadband Operation*

Single-ended channel estimation scheme discussed in the Section II provides frequency-resolved $\mathbf{H}(f)$ and enables broadband MIMO preprocessing. We set up a simulation model to characterize the performance of time reversal and present the results for two spatial and polarization modes, which can be two polarization states of a PMF. Concatenated model is usually applied for modeling optical fibers with strong modal dispersion through dividing the fiber into multiple sections [28]. For the sake of simplicity, we assume PMD only occurs at one section. This assumption has no impact on the broadband operation analysis and is valid for the experiment using a single PMF. The link is modeled as $\mathbf{H_{MD}} = \mathbf{UDV}$, where $\mathbf{U}$ and $\mathbf{V}$ are unitary matrices to represent random mode coupling introduced by the SMFs before and after the PMF, and $\mathbf{D}$ is a diagonal delay matrix representing the PMF where birefringence is introduced. Polarization-diversity 20-Gbaud Nyquist-shaped QPSK signal with a length of 2^{12} is transmitted and sampled at a rate of two samples per symbol. Channel estimation is operated in a sample basis. $\mathbf{H}(f)$ has a frequency range from -20 GHz to 20 GHz. Broadband time reversal is based on the MIMO preprocessing using $\mathbf{H^{-1}}(f)$. After broadband MIMO preprocessing and fiber propagation, the total matrix can be written as $\mathbf{H_{MD}H^{-1}}(f)$, whose four elements are H_{xx}, H_{xy}, H_{yx} and H_{yy}.

Fig. 6(a) shows the intensity for all the elements over the 40 GHz bandwidth as the polarization delay is 20 ps. Extinction

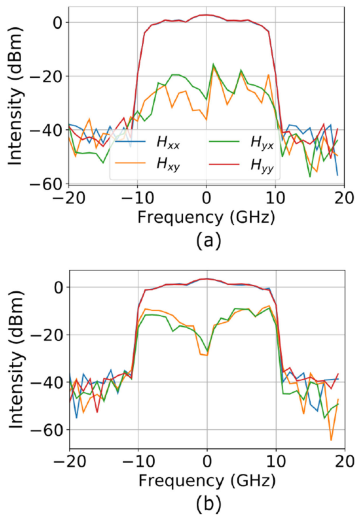

Fig. 7. Experimental results over a 5-m PMF propagation for the intensity of all four elements of (a) $\mathbf{H_{MD}H^{-1}}(f)$ as broadband MIMO preprocessing and (b) $\mathbf{H_{MD}H^{-1}}(f=0)$ as narrow-band MIMO preprocessing.

ratios (ER) between the two polarizations are more than 30 dB, which are consistent over the whole 20-GHz signal bandwidth (-10 to 10 GHz). Fig. 6(b) presents the results as only $\mathbf{H}^{-1}$ at the center frequency is employed in the MIMO preprocessing, which can be described as $\mathbf{H_{MD}H^{-1}}(f=0)$. In this case, a linear phase shift over the frequency cannot be compensated due to the 20-ps polarization delay so that the residual phase errors induce frequency-dependent ERs. ER is high at the center frequency but starts to degrade as the frequency offset enlarges. Polarization focusing employing only $\mathbf{H}^{-1}(f=0)$ is further degraded as the polarization delay is increased as to 40 ps, see Fig. 6(c).

In order to experimentally investigate the performance of broadband MIMO preprocessing over a fiber with a large modal dispersion, we chose a 5-m PMF and built a coherent transmission system with the same parameters as described in the simulation. The intensity of all four elements of measured $\mathbf{H_{MD}H^{-1}}(f)$ and $\mathbf{H_{MD}H^{-1}}(f=0)$ is present in Fig. 7(a) and (b). It is verified experimentally that with strong modal dispersion (PMD in this case) broadband transmitter-side MIMO preprocessing is inevitable to achieve spatial-temporal focusing as indicated by the simulation.

B. Focusing Over MMF

We use telecommunication techniques to calculate $\mathbf{H}$ over a large bandwidth remotely at the input employing coherent receivers and vector modulators. Fig. 8(c) shows the experimental setup for remote spatio-temporal focusing over an optical-wireless link consisting of a graded-index MMF supporting 6 spatial and polarization modes and half a meter of free space. To guarantee that 6-by-6 $\mathbf{H}$ is stable during the time period of the measurement, a 20-m MMF was used in the experiment. A tunable laser operating at C-band was modulated by an in-phase and quadrature (IQ) dual-polarization Mach-Zehnder modulator (DP-MZM) to generate a polarization-diversity quadrature phase shift keying (QPSK) or carrier-suppressed on-off keying (OOK) signal. The DP-MZM was driven by a 4-channel programmable digital-to-analog converter (DAC). A pair of mode-group selective SMUX with a better than -18-dB ER between the LP_{01} and LP_{11} mode groups were applied. Together with the fact that our 20-m MMF does not noticeably couple the LP_{01} to LP_{11} modes due to large effective refractive index difference, the high SMUX ER enables us to treat the mode control problem separately for the two LP_{01} modes and the four LP_{11} modes. The modulated light was amplified and launched into either the LP_{01} or the LP_{11} mode group through an optical switch. At the distal end, partial reflectors with 70% transmission were placed after SMUX_d with different time delays as spatial pilots. Reflected signal was sent back to the dual-polarization coherent receiver (Rx) at the proximal end through multiple optical circulators and captured by a 4-channel 50-GSamples/s digital sampling oscilloscope, see Fig. 8(b).

Channel estimation by multiplying the received reflected signal with the pseudo inverse of time-aligned transmitted training sequence was used to measure $\mathbf{H_D}(f)$ and $\mathbf{H}(f)$ is reconstructed digitally from $\mathbf{H_D}(f)$. After singled-ended channel estimation, transmitted signal was time reversed by multiplying frequency-resolved $\mathbf{H}^{-1}(f)$ and applied again to the DP-MZM, see Fig. 8(b). The frequency resolution of $\mathbf{H}(f)$ is inversely proportional to the training sequence duration, which is the pattern length times the symbol period. In the experiment, a 20-Gbaud QPSK signal with a length of 2^{12} is used as the training sequence for channel estimation, which can provide a finest frequency resolution around 5 MHz over the 20-GHz signal bandwidth to cope with intense modal dispersion. However, $\mathbf{H}(f)$ with a finer frequency resolution means more taps will be needed in the time-resolved $\mathbf{h}(t)$, which increases system's computational complexity. For the current setup, a frequency resolution of 2 GHz is sufficient and applied to resolve the modal dispersion of the 20-m MMF, which results in $\mathbf{h}(t)$ with only 20 taps.

Measured frequency-resolved $\mathbf{H}(f)$ of the LP_{01} modes is present in Fig. 9. Due to the strong coupling (0-dB off-diagonal elements), QPSK signal for both polarizations cannot be recovered without employing MIMO-based DSP at the receiver. The ER between LP_{01x} and LP_{01y} modes is significantly enhanced from -2.5 dB to better than -22 dB after transmitter-side MIMO preprocessing. To examine the frequency dependence of $\mathbf{H}$, we detuned the wavelength for mode-focusing from the wavelength where $\mathbf{H}(f)$ is measured by $\Delta\lambda$ and obtained the ER results shown in Fig. 10(a). It shows that ER dramatically degrades as the wavelength offset gets larger, which indicates the fast change of $\mathbf{H}$. MIMO preprocessing operation is transparent to the signal modulation format. Fig. 10(a) and (b) shows MIMO preprocessed transmission results for a Nyquist-shaped 20-GBaud QPSK signal with a spectral roll-off of 0.1 and a 10-Gbaud OOK signal, respectively. No DSP at the receivers is applied to the OOK signal, whose eye diagrams are directly captured using an oscilloscope. The recovery of the QPSK constellations only requires frequency and phase error compensation due to the random frequency drift between the two lasers at the transmitter and receiver.

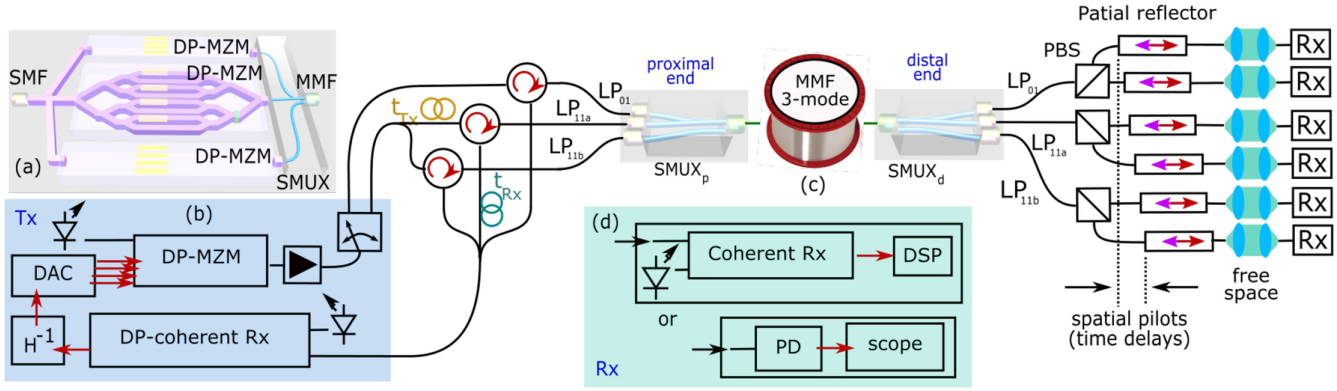

Fig. 8. (a) Schematic of transmitter-side MIMO processing employing an in-phase and quadrature (IQ) dual-polarization Mach-Zehnder modulator (DP-MZM) array, (b) transmitter (Tx) for $\mathbf{H}$ estimation and transmitter-side MIMO preprocessing, (c) setup of spatio-temporal focusing over MMF based on transmitter-side MIMO preprocessing, and (d) two sets of optical receivers (Rx) for receiving QPSK and OOK signal, respectively.

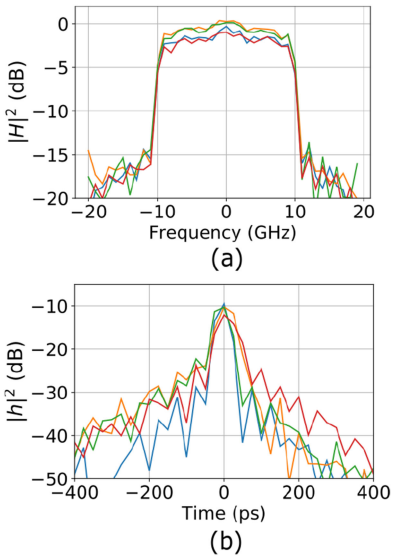

Fig. 9. Estimated $|\mathbf{H}|^2$ and $|\mathbf{h}|^2$ for the LP_{01} modes.

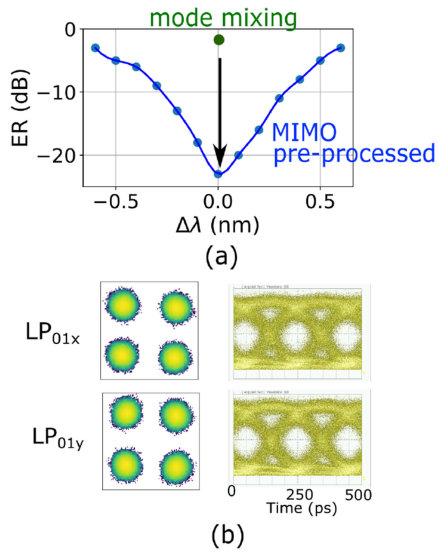

Fig. 10. (a) Extinction ratio (ER) between the LP_{01x} and LP_{01y} modes w/ and w/o transmitter-side MIMO preprocessing and wavelength detuning results, (b) constellations (left) and eye diagrams (right) for a focused QPSK and OOK signal.

The same transmitter was used to focus the four LP_{11} modes. Fiber delays t_{Tx} and t_{Rx} were added to differentiate input (launched) and output (reflected) modes in $\mathbf{H}$ estimation. A time-interleaving method [29] is applied to realize 4-by-4 MIMO preprocessing for the four LP_{11} modes employing only one IQ DP-MZM. MIMO preprocessed waveforms for the LP_{11a} and LP_{11b} modes are stitched in time, see Fig. 11(d). The relative amplitudes and phases between LP_{11a} and LP_{11b} are important for $\mathbf{H}^{-1}$ preprocessed mode forming. Proper results are only obtained by this technique when the signal processed for LP_{11a} is in the LP_{11a} mode while the signal processed for LP_{11b} is in the LP_{11b} mode (equal colors in Fig. 11(d)). Mode focusing expectedly fails when the mapping is reversed during time multiplexing. Practical systems would use individual modulators for each mode, eliminating the problem. As illustrated in Fig. 8(a), transmitter-side MIMO preprocessing of 6 spatial and polarization modes can be realized by 3 IQ DP-MZMs, which can be integrated into an array device [30] and co-packaged with the proximal-end 3D-waveguide (3DW) SMUX [31] to interface with an MMF.

Fig. 11(a) presents the intensity of $\mathbf{H}$ of the LP_{11} modes at different frequency offsets. Fig. 11(b) shows the summed intensity of $\mathbf{H}^{-1}$ over all the frequency bins used for MIMO preprocessing. Fig. 11(c) shows the 20-GBaud QPSK constellations for the four LP_{11} modes, which were focused at the distal output and detected individually. Similar to the LP_{01} case, only frequency and phase error compensation is applied for signal recovery. The lower portion of Fig. 11(d) shows the power per block measured in each mode as a function of time, indicating successful mode focusing with about 8-dB extinction. We used a scope with four channels to capture the output voltages from four photo-detectors, which detect the power of the four LP_{11} modes. The power fluctuations in the plot are caused by the difference between the scope's sampling speed and transmitted

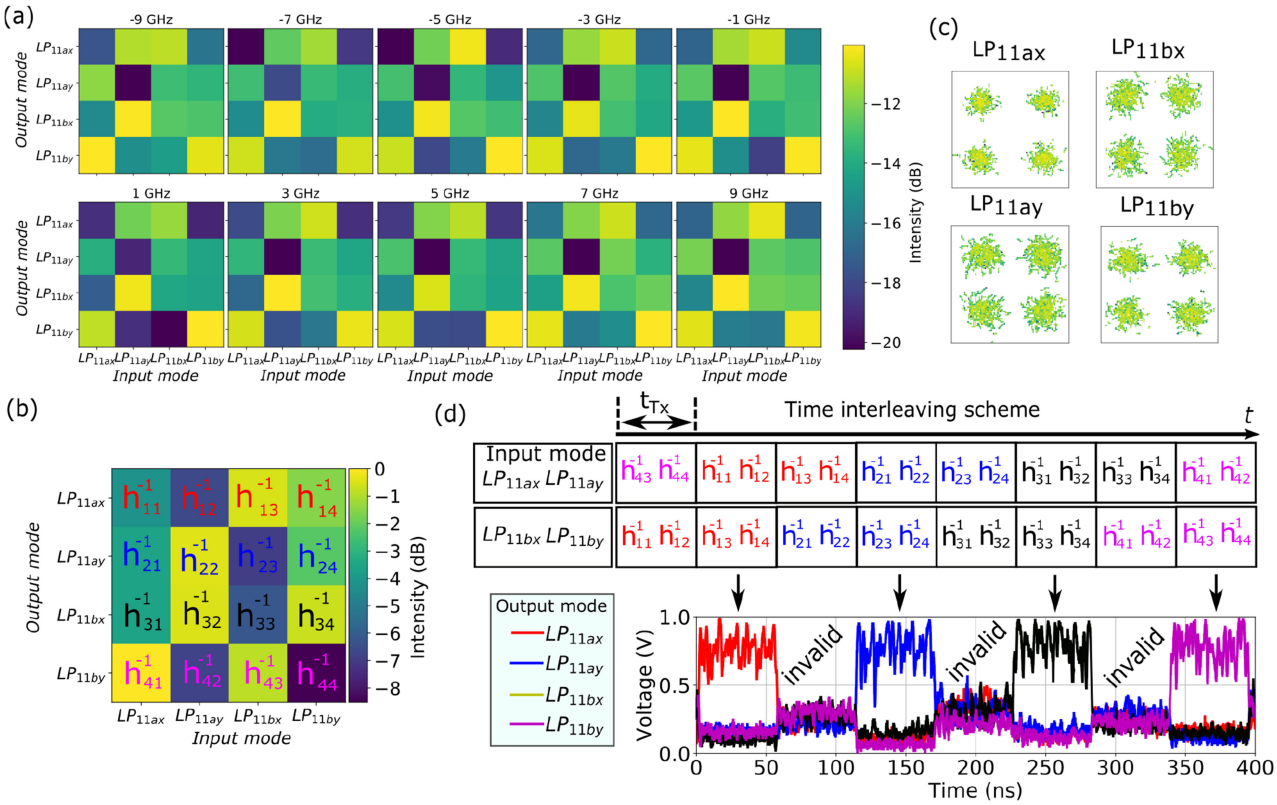

Fig. 11. (a) Intensity of the estimated $\mathbf{H}$ of the LP_{11} modes at different frequency offsets, (b) summed intensity of the $\mathbf{H^{-1}}$ over the whole bandwidth, (c) recovered QPSK constellations for all the LP_{11} modes, and (d) each mode is being focused at the distal end sequentially based on the time-interleaving scheme and 4-by-4 MIMO preprocessing.

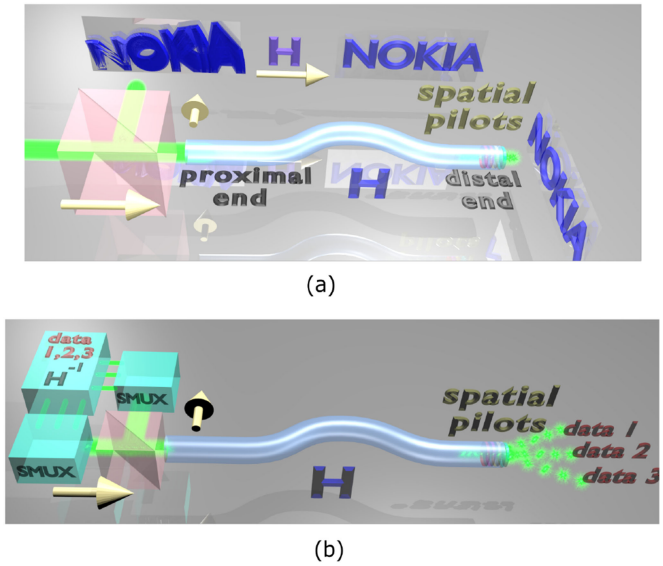

Fig. 12. Single-ended channel estimation enabled perturbation-insensitive remote mode-forming applied for (a) ultra-thin fiber endoscopy and (b) passive optical network with lossless beam combining and splitting.

signal's symbol rate. Residual crosstalk is caused partially by the mode-dependent loss from the SMUX and the nonlinear response of the DP-MZM, which can be reduced by further optimization.

IV. Conclusion

Remote spatio-temporal focusing over an MMF was experimentally demonstrated employing single-ended channel estimation and broadband transmitter-side MIMO processing. We believe that the proposed single-ended channel estimation scheme can enable perturbation-insensitive remote mode-forming applied for biophotonics and telecommunication, such as ultra-thin fiber endoscopy and passive optical network with lossless beam combining and splitting, as illustrated in Fig. 12. Although we performed this measurement over 6 spatial modes, we view this as a starting point for 100 s of modes due to the availability of mode multiplexers supporting more than 200 spatial modes [32], [33] and demonstrations of integrated devices [34] to maintain distal end compact.

In the demonstration, channel estimation and transmitter-side MIMO processing is done off-line, which makes it challenging to cope with fast varying optical channels. To monitor much longer or more dynamically changed optical fiber, field-programmable gate array (FPGA)-based real-time transceivers will be preferred to use and large dimension real-time MIMO-DSP has been demonstrated for space division multiplexing applications [35].

Ultrashort pulses, often in the range of femtoseconds, have enormous applications, especially in biophotonics. Using MMF to deliver ultrashort pulses has been a hot research topic recently [20]. Transmitter-side MIMO preprocessing relies on telecommunication techniques. The smallest symbol period,

which is equivalent to pulse width, is determined by the bandwidth of the optical modulator. It is around 100 ps in the demonstration. In order to generate shorter pulses, optical modulators with larger bandwidth can be chosen [36]. An alternative way to create femto-second pulses is employing an optical spectrally sliced transmitter, which can use the bandwidth of multiple optical modulators [37].

REFERENCES

[1] Y. Choi *et al.*, "Scanner-free and wide-field endoscopic imaging by using a single multimode optical fiber," *Phys. Rev. Lett.*, vol. 109, no. 20, Nov. 2012, Art. no. 203901.

[2] M. Plöschner, T. Tyc, and T. Čižmár, "Seeing through chaos in multimode fibres," *Nature Photon.*, vol. 9, no. 8, pp. 529–535, Aug. 2015.

[3] S. Ohayon, A. Caravaca-Aguirre, R. Piestun, and J. J. DiCarlo, "Minimally invasive multimode optical fiber microendoscope for deep brain fluorescence imaging," *Biomed. Opt. Express*, vol. 9, no. 4, pp. 1492–1509, Apr. 2018.

[4] S. A. Vasquez-Lopez *et al.*, "Subcellular spatial resolution achieved for deep-brain imaging in vivo using a minimally invasive multimode fiber," *Light: Sci. Appl.*, vol. 7, no. 1, pp. 1–6, Dec. 2018.

[5] S. Turtaev, I. T. Leite, T. Altwegg-Boussac, J. M. P. Pakan, N. L. Rochefort, and T. Čižmár, "High-fidelity multimode fibre-based endoscopy for deep brain in vivo imaging," *Light: Sci. Appl.*, vol. 7, no. 1, pp. 1–8, Nov. 2018.

[6] R. G. H. v. Uden, C. M. Okonkwo, H. Chen, H. d. Waardt, and A. M. J. Koonen, "Time domain multiplexed spatial division multiplexing receiver," *Opt. Express*, vol. 22, no. 10, pp. 12 668–12 677, May 2014.

[7] N. K. Fontaine *et al.*, "30 × 30 mimo transmission over 15 spatial modes," in *Proc. Opt. Fiber Commun. Conf., Paper Th5C.1*, Mar. 2015, Paper. Th5C.1.

[8] J. Carpenter, B. C. Thomsen, and T. D. Wilkinson, "Degenerate mode-group division multiplexing," *J. Lightw. Technol.*, vol. 30, no. 24, pp. 3946–3952, Dec. 2012.

[9] B. Franz and H. Bülow, "Mode group division multiplexing in graded-index multimode fibers," *Bell Labs Tech. J.*, vol. 18, no. 3, pp. 153–172, Dec. 2013.

[10] C. Xia *et al.*, "Time-division-multiplexed few-mode passive optical network," *Opt. Express, OE*, vol. 23, no. 2, pp. 1151–1158, Jan. 2015.

[11] I. M. Vellekoop and A. P. Mosk, "Focusing coherent light through opaque strongly scattering media," *Opt. Lett.*, vol. 32, no. 16, pp. 2309–2311, Aug. 2007.

[12] T. Čižmár and K. Dholakia, "Shaping the light transmission through a multimode optical fibre: Complex transformation analysis and applications in biophotonics," *Opt. Express*, vol. 19, no. 20, pp. 18 871–18 884, Sep. 2011.

[13] R. N. Mahalati, D. Askarov, J. P. Wilde, and J. M. Kahn, "Adaptive control of input field to achieve desired output intensity profile in multimode fiber with random mode coupling," *Opt. Express*, vol. 20, no. 13, pp. 14 321–14 337, Jun. 2012.

[14] L. Büttner, D. Haufe, N. Koukourakis, and J. W. Czarske, "Transmission of individual optical signals through a multimode fiber using digital optical phase conjugation," in *Frontiers Opt.*, Oct. 2016, Paper. FF1G.3.

[15] I. N. Papadopoulos, S. Farahi, C. Moser, and D. Psaltis, "Focusing and scanning light through a multimode optical fiber using digital phase conjugation," *Opt. Express*, vol. 20, no. 10, pp. 10 583–10 590, May 2012.

[16] G. Lerosey, J. de Rosny, A. Tourin, A. Derode, G. Montaldo, and M. Fink, "Time reversal of electromagnetic waves," *Phys. Rev. Lett.*, vol. 92, no. 19, May 2004, Art. no. 193904.

[17] A. P. Mosk, A. Lagendijk, G. Lerosey, and M. Fink, "Controlling waves in space and time for imaging and focusing in complex media," *Nature Photon.*, vol. 6, no. 5, pp. 283–292, May 2012.

[18] M. Piels, E. P. Da Silva, J. Estaran, R. Borkowski, I. T. Monroy, and D. Zibar, "Focusing over optical fiber using time reversal," *IEEE Photon. Technol. Lett.*, vol. 27, no. 6, pp. 631–634, Mar. 2015.

[19] F. v. Beijnum, E. G. v. Putten, A. Lagendijk, and A. P. Mosk, "Frequency bandwidth of light focused through turbid media," *Opt. Lett.*, vol. 36, no. 3, pp. 373–375, Feb. 2011.

[20] E. E. Morales-Delgado, S. Farahi, I. N. Papadopoulos, D. Psaltis, and C. Moser, "Delivery of focused short pulses through a multimode fiber," *Opt. Express*, vol. 23, no. 7, pp. 9109–9120, Apr. 2015.

[21] M. Mounaix, H. Defienne, and S. Gigan, "Deterministic light focusing in space and time through multiple scattering media with a time-resolved transmission matrix approach," *Phys. Rev. A*, vol. 94, no. 4, Oct. 2016, Art. no. 041802.

[22] R. Y. Gu, R. N. Mahalati, and J. M. Kahn, "Design of flexible multi-mode fiber endoscope," *Opt. Express*, vol. 23, no. 21, pp. 26 905–26 918, Oct. 2015.

[23] H. Chen, N. K. Fontaine, R. Ryf, S. Chandrasekhar, B. Huang, and P. Winzer, "Beam-forming transmission enabled by transmitter-side MIMO using spatial pilots," in *Proc. Eur. Conf. Opt. Commun.*, Sep. 2017, pp. 1–3.

[24] H. Chen *et al.*, "Remote mode-forming over multimode fiber employing single-ended channel estimation," in *Proc. Eur. Conf. Opt. Commun.*, Sep. 2018, pp. 1–3.

[25] N. K. Fontaine *et al.*, "Characterization of space-division multiplexing systems using a swept-wavelength interferometer," in *Proc. Opt. Fiber Commun. Conf. Expo. Nat. Fiber Opt. Engineers Conf.*, Mar. 2013, pp. 1–3.

[26] L. Gruner-Nielsen *et al.*, "Few mode transmission fiber with low dgd, low mode coupling, and low loss," *J. Lightw. Technol.*, vol. 30, no. 23, pp. 3693–3698, Dec. 2012.

[27] B. Huang *et al.*, "All-fiber mode-group-selective photonic lantern using graded-index multimode fibers," *Opt. Express*, vol. 23, no. 1, pp. 224–234, Jan. 2015.

[28] K.-P. Ho and J. M. Kahn, "Statistics of group delays in multimode fiber with strong mode coupling," *J. Lightw. Technol.*, vol. 29, no. 21, pp. 3119–3128, Nov. 2011.

[29] D. J. Geisler *et al.*, "Bandwidth scalable, coherent transmitter based on the parallel synthesis of multiple spectral slices using optical arbitrary waveform generation," *Opt. Express*, vol. 19, no. 9, pp. 8242–8253, Apr. 2011.

[30] A. Hosseini *et al.*, "Extended C-band tunable multi-channel InP-based coherent receiver PICs," *Opt. Express*, vol. 25, no. 16, pp. 18 853–18 862, Aug. 2017.

[31] S. Gross, N. Riesen, J. D. Love, and M. J. Withford, "Three-dimensional ultra-broadband integrated tapered mode multiplexers," *Laser Photon. Rev.*, vol. 8, no. 5, pp. L81–L85, 2014.

[32] N. K. Fontaine, R. Ryf, J. Bland-Hawthorn, and S. G. Leon-Saval, "Geometric requirements for photonic lanterns in space division multiplexing," *Opt. Express*, vol. 20, no. 24, pp. 27 123–27 132, Nov. 2012.

[33] N. K. Fontaine, R. Ryf, H. Chen, D. T. Neilson, K. Kim, and J. Carpenter, "Laguerre-Gaussian mode sorter," *Nature Commun.*, vol. 10, no. 1, pp. 1–7, Apr. 2019.

[34] H. Chen, R. v. Uden, C. Okonkwo, and T. Koonen, "Compact spatial multiplexers for mode division multiplexing," *Opt. Express*, vol. 22, no. 26, pp. 31 582–31 594, Dec. 2014.

[35] S. Randel *et al.*, "First real-time coherent MIMO-DSP for six coupled mode transmission," in *Proc. IEEE Photon. Conf.*, Oct. 2015, pp. 1–2.

[36] Y. Ogiso *et al.*, "Over 67 GHz bandwidth and 1.5 V Vpi InP-based optical IQ modulator with n-i-p-n heterostructure," *J. Lightw. Technol.*, vol. 35, no. 8, pp. 1450–1455, Apr. 2017.

[37] B. Guan *et al.*, "Optical spectrally sliced transmitter for high fidelity and bandwidth scalable waveform generation," *J. Lightw. Technol.*, vol. 34, no. 2, pp. 737–744, Jan. 2016.

Haoshuo Chen received the Ph.D. degree (*cum laude*) in electrical engineering from the Eindhoven University of Technology (TU/E), Eindhoven, The Netherlands, in 2014. Since December 2014, he has been a Technical Staff Member with Nokia Bell Labs, Holmdel, NJ, USA. His main research interests include space division multiplexing for telecommunication and imaging, dense photonic integration, power efficient digital signal processing, fiber components, and wavelength/space switches.

Nicolas K. Fontaine received the Ph.D. degree in electrical engineering from Next Generation Network Systems Laboratory, University of California, Davis, CA, USA, in 2010. In his dissertation, he studied how to generate and measure the amplitude and phase of broadband optical waveforms in many narrowband spectral slices. Since June 2011, he has been a Technical Staff Member with Advanced Photonics Division, Bell Laboratories, Crawford Hill, NJ, USA. At Bell Labs, he develops devices for space-division multiplexing in multi-core and few mode fibers, builds wavelength crossconnects and filtering devices, and investigates spectral slice coherent receivers for THz bandwidth waveform measurement.

Roland Ryf received the Diploma and the Ph.D. degree in physics from the Swiss Federal Institute of Technology, Zürich, Switzerland, where he was involved in photorefractive self-focusing and spatial solitons, parallel optical processing based on holographic storage, and fast optical correlation. Since May 2000, he has been a member of the Photonic Subsystems and the Advanced Photonics Research Department, Bell Laboratories, Alcatel-Lucent, Holmdel, NJ, where he is involved in the optical design and prototyping of optical microelectromechanical systems (MEMS) and liquid crystal on silicon-based devices. In particular, he has been involved in large port count cross-connect switches, programmable high-resolution spectral filters, wavelength selective switches, MEMS-based infrared sensors, and laser projection displays. He has been most recently involved in the free-space couplers and optical transmission in multicore and multimode fibers. He has more than 60 publications and more than 15 patents in the field of optical communication.

David T. Neilson (Fellow, IEEE) received the B.Sc. and Ph.D. degrees in physics from Heriot-Watt University, Edinburgh, U.K., in 1990 and 1993, respectively. His doctoral thesis was on "Optical Nonlinearities and Switching in InGaAs Quantum Wells." From 1993 to 1996, he was a Postdoctoral Researcher working on free-space optical interconnect and switching systems with Heriot-Watt. From 1996 to 1998, he was a Visiting Scientist with NEC Research, Princeton, NJ, researching optical interconnects for high-performance computing systems. In 1998, he joined Bell-Labs, where he has researched several optical switching systems and technologies including using micro-mechanical elements and LCoS for wavelength selective switches and optical crossconnects. He has also led groups working on InP optoelectronic growth and fabrication and Silicon photonics. He has authored more than 200 publications, patents, and short courses, on both devices and systems in the field of optical interconnects and switching. He has served on and chaired several IEEE-LEOS, OSA, and SPIE conference programs in the field of optical interconnects and switching. He is a Bell Labs Fellow.

Peter Winzer (Fellow, IEEE) received the Ph.D. degree in electrical engineering from the Technical University of Vienna, Vienna, Austria, in 1998. Supported by the European Space Agency, he investigated space-borne Doppler lidar and laser communications. Since 2000, he was with Bell Labs, where he has focused on fiber-optic communication systems and networks and has contributed to high-speed optical transmission records and product developments from 10 Gb/s to 1 Tb/s per carrier. Following his involvement in estimating the nonlinear fiber Shannon capacity, he investigated space-division multiplexing and multiple-input-multiple-output techniques for fiber-optics and is globally promoting SDM to scale optical transport systems. He currently heads Bell Labs' global Optical Transmission Research efforts. He has widely authored/coauthored and patented and is actively involved with the IEEE and the Optical Society of America (OSA). He was the Editor-in-Chief for the *Journal of Lightwave Technology* from 2013 to 2018, was a Program Chair of the 2009 European Conference on Optical Communications and Program/General Chair of the 2015/2017 Optical Fiber Communication Conference. He is a Bell Labs Fellow, a fellow of the OSA, and an Elected Member of the U.S. National Academy of Engineering. He has received multiple awards for his work, including the 2018 John Tyndall Award.